

Differential Scanning Calorimetry and Electrochemical Tests for the Analysis of Delamination of 3PE Coatings

Qiao Weibiao^{1,*}, Li Bingfan², Kang Zhangyang¹

¹ North China University of Water Resource and Electric Power, China;

² China University of Petroleum (East China), China

*E-mail: qwb201710@163.com

Received: 12 October 2018 / Accepted: 27 May 2019 / Published: 30 June 2019

In order to identify the causes of coating delamination on buried pipelines, a field test was conducted to determine the environmental condition of delaminated coatings, and then an electrochemical test and DSC were used to find the cause of delamination. The results show that the main cause of delaminated coatings with defects is the diffusion of electrolyte on the coating and metal interface, which can be divided into three stages, the formation of corrosive crevice, oxygen concentration corrosion, and the hydrogen evolution process. In addition, based on the physical meaning of EECs, the correlation between $f_{\theta_{\max}}$ and all other parameters was established. The result of DCS demonstrates that lacking the cross-linking density of epoxy can also result in delamination of 3PE coatings.

Keywords: 3PE anti-corrosive coating; Delamination; Cathodic protection; Coating/metal interface; Glass transition temperature

1. INTRODUCTION

The combination of cathodic protection and coatings is commonly used for anti-corrosion of buried pipelines. Coatings as the first line [1] of anti-corrosion isolate pipelines from corrosive medium, and also greatly protect pipelines from mechanical damage [2]. However, under some circumstances, delamination of coatings occurs, which may result in remarkable financial loss. Coating failures can occur for many reasons. Typical causes include poor applications, defective coatings [3], pitting corrosion, development of residual stresses, inadequate specifications, etc. [4]. It is critical to determine the root causes of coating failures. Not only does this help avoid financial loss but also is often the first step to solve the problem.

In general, there may be four causes of delamination of 3PE coatings (Fused epoxy - extruded polyethylene structural protective coating, that consists of three layers, named as fused epoxy, adhesive

substance and extruded polyethylene, respectively). First, due to mechanical damage, some defects on the surface of coatings make pipelines directly exposed to the soil. Under this circumstance, hydrogen evolution reaction or corrosion may occur induced by stray current in soil, and then corrosion crevice is gradually formed and transports along pipelines, resulting in delamination [5]. Second, if the PE layer is damaged, the water or electrolyte in the soil diffuses in the epoxy layer, and an electrochemical reaction occurs when it reaches the coating and metal interface, and then the alkaline environment and the accumulation of corrosion products may destroy the bonding force between the coating and metal, causing delamination [6]. Third, because of the interference of ultra-high voltage power transmission, vigorous fluctuations of potential of buried pipelines may directly destroy the coatings. Lastly, non-conformity of coatings may lead to insufficient adhesion between coatings and pipelines, leading in delamination [7].

To investigate and analyze the conditions that cause the failure, data of failed coatings must be collected, including the coating types, application procedures, service history and environment, and physical evidence. The data is used to determine why, how, when and where a failure may occur [8]. Therefore, in this paper, a field test was first conducted to determine the environment delaminating coatings, and then an electrochemical test and differential scanning calorimetry (DSC) were used to explore the causes of delamination. Understanding the causes of failure is necessary to prevent future coating failures

2. EXPERIMENTAL SECTION

There were two types of delamination with and without defects in coatings found in the field test. In the environment with a water content higher than 50%, at the location of stripped coatings with defects, its cathodic protection potential of $-0.974\sim-1.36V_{VS.CSE}$ meets the requirements [9]. Therefore, the electrolyte diffusion on the coating and metal interface from the defects may result in delamination. On the other hand, as shown in Figure 1, for the delaminated coating without defects, there is little corrosion products on the surface of the pipeline. Hence, the delamination could be caused by insufficient cured epoxy. Based on above analysis, this paper employs the electrochemical test and DSC analysis to identify the causes of delamination [10].



Figure 1. Pictures of delaminated coating without defects in field

In this paper, to explore the electrochemical reaction on the interface, an artificial defect with a diameter of 6.4mm was created, as shown in Figure 2. From bottom to top, the 3PE coatings consist of three layer of fused epoxy, adhesive substance and extruded polyethylene (PE), which thickness is 123 μm , 184 μm and 2.1mm, respectively. And the substrate metal is X65 steel. The process for preparing the 3PE samples is described as follows. Firstly, the temperature of X65 steel is heated to 190~210 $^{\circ}\text{C}$, and then the epoxy and adhesive layer are successively laid by electrostatic spraying. Thirdly, lay PE layer and quickly remove the specimen to cool through spraying water to room temperature. After the preparation is completed, digital engraving machine is applied to drill the holes with diameter 6.4mm. Except for the artificial defect, the rest part is covered with a PE layer that can keep intact in a long immersion, hence, diffusion in the normal direction can be ignored. In this experiment, the cathodic protection potential of -1.0V_{vs.CSE} was applied and EIS was conducted over the frequency range from 100kHz up to 10mHz using an electrochemical working station PARSTAT2273. The measurements were performed using a 10mV voltage amplitude. A PVC tube with an inner diameter of 75mm was clamped onto the 3PE coated metal and was subsequently filled with the wt.3.5% NaCl solution. This experiment was conducted at the constant temperature of 25 $^{\circ}\text{C}$ in an oven GDJS-408. The equivalent electric circuits were fitted by ZSimpWin software [11].

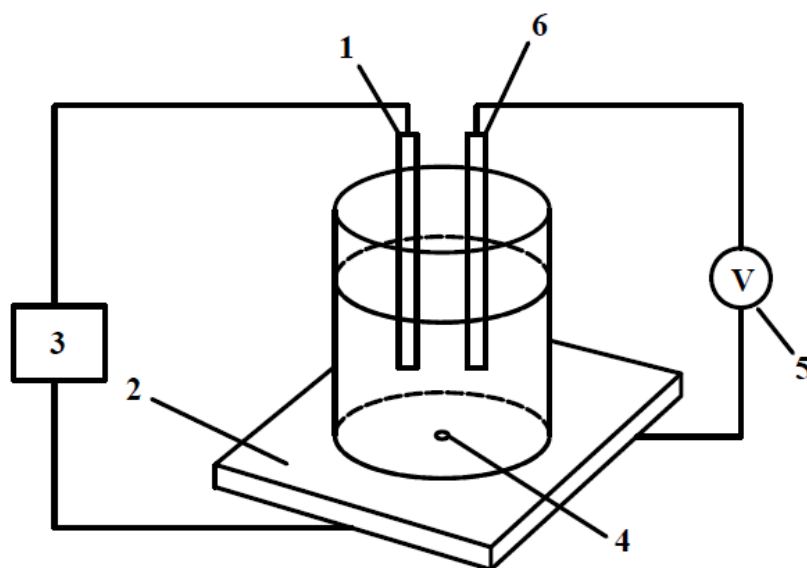


Figure 2. Experimental design of EIS on coating/metal interface under cathodic protection 1-Pt as auxiliary electrode and SCE as reference electrode; 2-PE layer; 3-Electrochemical working station PARSTAT2273; 4-An artificial defect with diameter 6.4mm;5-Cathodic protection devices; 6-Pt as anodic electrode

3. RESULTS AND DISCUSSION

3.1 Analysis of diffusion on coating and metal surface

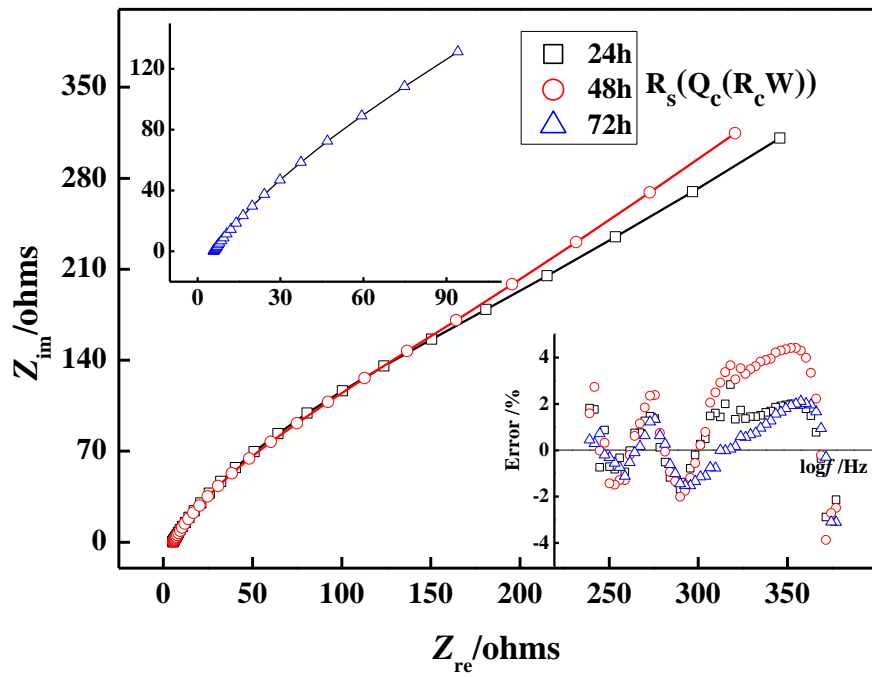
Figure 3 shows the tested curves of EIS over time. The fitted results of equivalent electric circuits were also obtained and shown in Table 1. It is obvious to observe that the entire process of diffusion on the coating and metal surface can be divided into three stages.

The first stage is in the timeframe of 0 to 72h. It can be seen that at 24h, the Nyquist plots can be described by the combination of capacitive resistance and diffusion impedance. The presence of the diffusion resistance indicates that the electrolyte has gradually spread into the interface. Under the cathodic protection, oxygen reaction dominates in the near-neutral pH solution, that is, in cathode: $O_2+2H_2O+4e^- \rightarrow 4OH^-$; in anode: $Fe \rightarrow Fe^{2+}+2e^-$. Therefore, this stage is dominated by the oxygen depolarization reaction and electrolyte diffusion on the interface to form corrosion crevice. At this moment, the capacitance of the coating Q_c increases as resistance R_c decreases, and the diffusion resistance Z_w performs a non-ideal Warburg resistance at $n \approx 0.75$ [12]. However, as the reaction lasts to 72h, while there is still a tail of diffusion resistance [13,14], the diameter of the capacitance resistance arc decreases obviously. The tail illustrates that the oxygen in crevice is gradually exhausted [15,16], and the electric double layer is progressively formed. In addition, the time constant $\tau=C_c \cdot R_c$ basically remains unchanged.

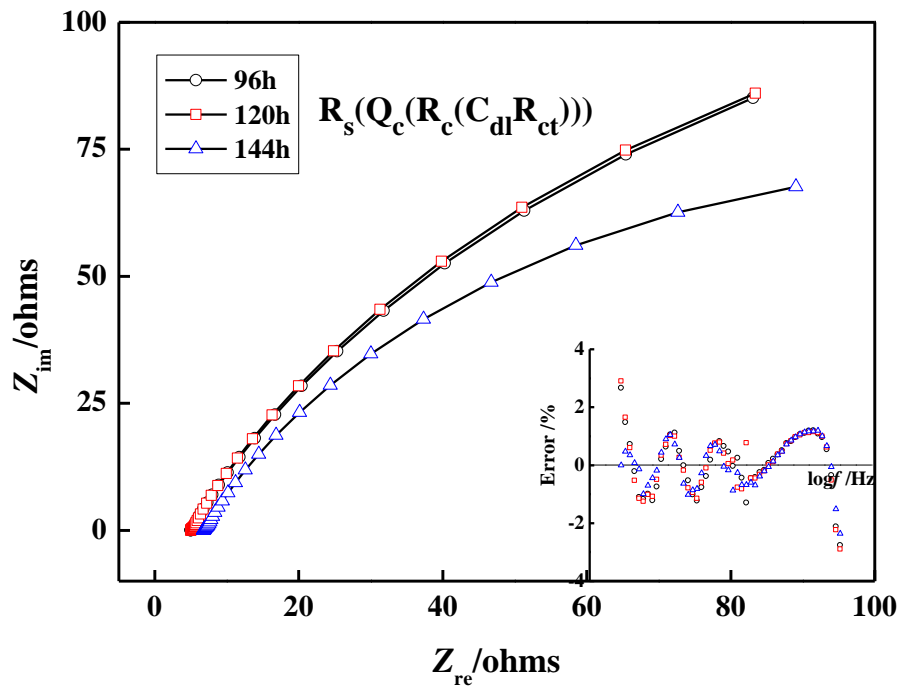
The second stage is from 72h to 144h. When the experiment is undergone to the time of 96h, the diffusion impedance disappears completely and corrosion crevice is formed. Because of the un gated characteristic of corrosion crevice, external oxygen is difficult to permeate to the corrosion front. Therefore, the oxygen concentration cell goes into the point outside of crevice and works as cathode while the cell inside of crevice is identified as anode. Consequently, the dissolution and hydrolysis of metal occur in the crevice front: $Fe+2H_2O \rightarrow Fe(OH)_2+2H^++2e^-$. Within the subsequent 36h, oxygen concentration corrosion dominates the whole process. At this stage, the time constant stays the same magnitude order [17].

As the test time goes to the 168h, obvious Warburg diffusion occurs with $n \approx 0.5$. Under the cathodic protection, based on the theory of IR drop [18,19], the hydrogen evolution reaction on the crevice front may occur: $H_2O+e^- \rightarrow H_{ad}+OH^-$. Therefore, the adsorption of H_{ad} on the surface of metal takes place and the diffusion layer of H_{ad} results in the appearance of Warburg resistance. In this stage, charge transfer resistance R_{ct} decreases and capacitance of the double electric circuit C_{dl} increases.

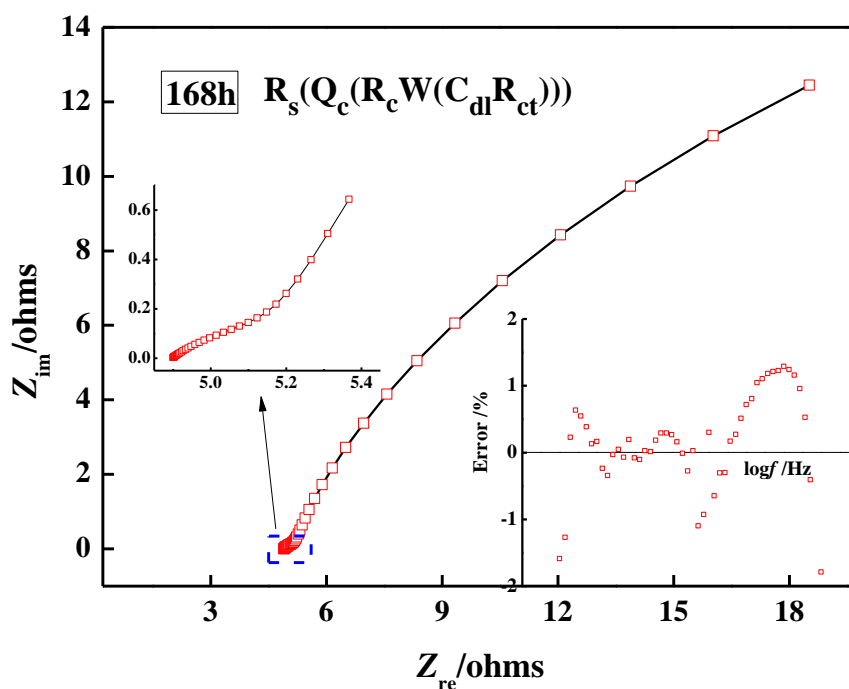
Based on the above analysis, the entire process can be divided into three stages. First, the electrochemical reaction is mainly oxygen depolarization and then corrosion crevice is gradually formed. Next, once the crevice is formed, due to the feature of crevice, oxygen concentration cells enter into being, and dissolution and hydrolysis of metal occurs in the crevice front. Then, with the cathodic protection and without oxygen, hydrogen evolution reaction may occur [20].



(1) First stage of 0~72h



(2) Second stage of 72h~144h



(3) Third stage of 144h~168h

Figure 3. Equivalent electric circuits and error analysis over test time

At this moment, the physical structure is under the un gated and electrochemical reaction conditions, which include insufficient oxygen, the presence of water and cathodic protection, and being located at the crevice front. Those conditions provide an environment for water to permeate into the coating. Hence, when water in soil diffuses to the coating and metal interface, the hydrogen evolution reaction [21] occurs due to the accumulation of hydrogen resulting from the cathodic protection, which may lead to stress concentration and delamination of coatings.

Table 1. Fitted results of equivalent electric circuits

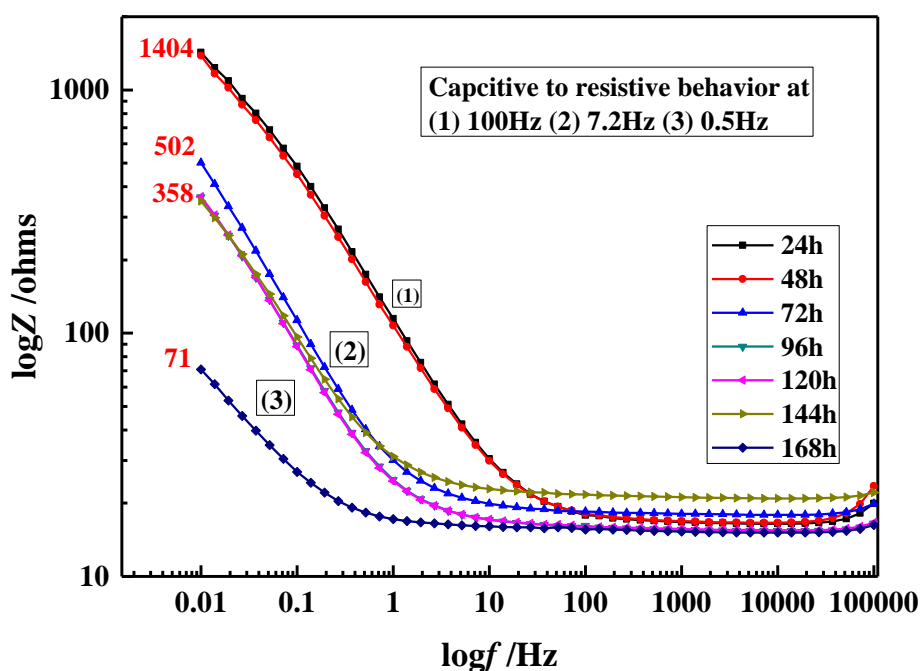
Time		24h	48h	72h	96h	120h	144h	168h
Parameter	R_s	5.36	5.54	5.85	4.98	5.01	6.77	4.90
	(Ω)	0.78	1.54	0.37	0.38	0.38	0.31	0.52
Q_c	Value/ 10^{-2}	0.70	0.73	4.17	4.60	4.65	4.40	17.71
	(F/cm^2)	2.91	6.911	1.32	3.37	3.43	3.00	13.26
n	Value	0.7535	0.78	0.77	0.70	0.71	0.71	0.55
	Error/%	1.14	2.61	0.92	1.64	1.56	1.40	8.75
R_c	Value	299.50	236.00	243.90	2.30	2.67	4.19	0.49
	(Ω)	11.77	18.64	12.66	18.59	19.28	11.50	10.74
Z_w	Value/ 10^{-2}	0.88	0.80	1.62	-	-	-	80.00
	(Ω)	6.50	10.39	19.61	-	-	-	16.99
C_{dl}	Value/ 10^{-2}	-	-	-	0.83	0.85	0.868	11.99
	(F/cm^2)	-	-	-	18.89	18.94	20.03	14.46
R_{ct}	Value	-	-	-	342.8	334.6	217.7	59.19
	(Ω)	-	-	-	6.246	5.845	3.729	22.85

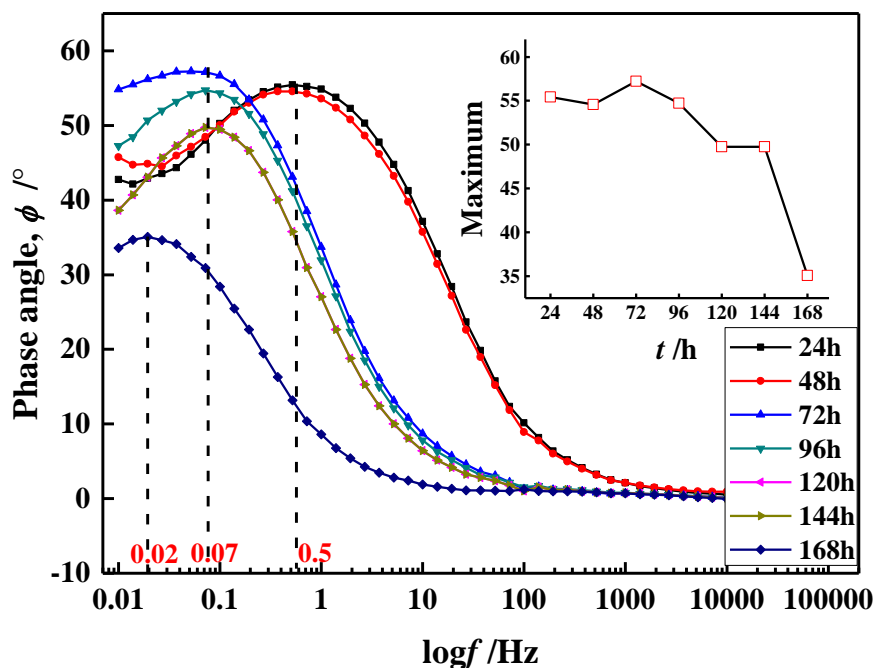
Figure 4 shows the relationships between $\log f$ and $\log Z$, and $\log f$ and the phase angle respectively. The curves show the similar regulations to the analyzed results of Nyquist plots. Those curves also demonstrate that the whole diffusion process can be divided into three stages.

In the first stage of 0~48h, at $f=0.5\text{Hz}$, the phase angle reaches the peak value of 55° , rather than 90° . It indicates that a non-ideal capacitance exists in the region of low frequency, which agrees with the analysis in Nyquist plots with $n \approx 0.75$. Two aspects lead to this phenomenon. One is the occurrence of diffusion on the coating and metal interface, and another is the existence of the artificial damaged defect. The combination of the two aspects makes the characteristics deviate from the pure capacitance, and leads to the phase angle deviating from 90° in the initial stage.

In the second stage of 48h~144h, the frequency of the maximal phase angle reduces to 0.07Hz. Even though the maximal phase angle at 72h is slightly larger than that at 48h, as test time goes by, the maximal phase angle gradually decreases. It proves that the corrosion crevice and double electric layer are formed [22], which is consistent with the aforementioned analysis.

In the third stage of 144h~168h, the frequency of the maximal phase angle reduces to 0.02Hz, and the maximal phase angle reduces to 35° . The frequency of capacitance turning into resistance transforms from 100Hz to 0.5Hz, and the charge transfer resistance decreases from 1404Ω to 71Ω . At this moment, the double electric layer is formed. Due to the adsorption of H_{ad} generated by the hydrogen evolution reaction, the mass transfer process gradually replaces the charge transfer process [23].





(2) $\log f-\phi$

Figure 4. Curves of resistance and phase angle in frequency

Isao Sckine et al. [24] proposed that the frequency of the maximal phase angle, named as $f_{\theta_{max}}$, can be used to evaluate the performance of coatings. At the beginning of water permeation, the equivalent electric circuits (EECs) of coatings can be described by $R_s(C_cR_c)$. Under this condition, the $f_{\theta_{max}}$ is in a linear relationship with R_c . Considering the dispersion effect, the relationship between $f_{\theta_{max}}$ and R_c is expressed by Eq.(1):

$$\log(f_{\theta_{max}}) = -\log 2\pi - 0.5\log(R_s C_c^2) - 0.5\log(R_c) \tag{1}$$

Table 2 presents the calculation results and errors of $f_{\theta_{max}}$ and R_c using Eq.(1). Except for the point at 72h, $f_{\theta_{max}}$ and R_c have good consistency. Therefore, $f_{\theta_{max}}$ can be applied to evaluate the characteristic of coatings to study water permeating into coatings or research the failure process due to diffusion on the coating and metal interface,

However, it should be noted in Table 2 that there are unacceptable errors of R_c and $\log(f_{\theta_{max}})$ calculated by Eq.(1). This is due to neglecting the impact of other parameters on $f_{\theta_{max}}$. Therefore, in this section, based on the physical meaning of EECs, the correlation between $f_{\theta_{max}}$ and all other parameters is established.

In the first stage, comparing Eq.(1) with the EECs, the error is derived from neglecting the influence of the dispersion coefficient in Eq.(1). Hence, the modified equation can be described as follows [25,26]:

$$\log(f_{\theta_{max}}) = -\log 2\pi - 0.5\log(R_s Q^2 / n) - 0.5\log(R_c) \tag{2}$$

In the second stage, the corrosion crevice and double electric layer are gradually formed. Therefore, the feature of the double electric layer must have a great influence on $f_{\theta_{max}}$. It should be noted that R_{ct} is different from R_c because it is mainly affected by the charge transfer process in high frequency.

Table 2. Relationship and calculated error of $f_{\theta_{max}}$ and R_c using Eq.(1)

Time	$f_{\theta_{max}}$	R_c	$\log(f_{\theta_{max}})$	Calculation	Error/%
24h	0.50	299.50	-0.30	-0.25	-18.46
48h	0.50	236.00	-0.30	-0.22	-26.33
72h	0.07	243.90	-1.15	-0.99	-13.85
96h	0.07	2.23	-1.15	0.01	-100.90
120h	0.07	2.67	-1.15	-0.03	-97.48
144h	0.07	2.42	-1.15	-0.05	-95.79
168h	0.02	0.49	-1.70	-0.23	-86.18

It can be seen in the range of high frequency from Figure 4(1) that R_{ct} is almost a constant, which indicates that R_{ct} is not impacted by the test frequency [27]. Hence, the maximal phase angle in $R_c(C_{dl}R_{ct})$ of the double electric layer, named as $f'_{\theta_{max}}$, can be described as follows:

$$\log(f'_{\theta_{max}}) = -\log 2\pi - 0.5\log(R_c C_{dl}^2) - \log R_{ct} \tag{3}$$

As a result, the $f_{\theta_{max}}$ for total EECs of $R_s(Q_c(R_c(C_{dl}R_{ct})))$ can be described as :

$$\begin{aligned} \log(f_{\theta_{max}}) &= -\log 2\pi - 0.5\log(R_s Q^2 / n) + \log(f'_{\theta_{max}}) \\ &= -\log 2\pi - 0.5\log(R_s Q^2 / n) + (-\log 2\pi - 0.5\log(R_c C_{dl}^2) - \log R_{ct}) \end{aligned} \tag{4}$$

As mentioned above, Eq.(4) can also be used to describe the third stage.

Table 3 shows the calculation results and errors using Eq.(2) and Eq.(4). It can be seen that the maximal error is less than 20%, showing a better consistency. The error existing in new equations includes the systematic error and fitting error of the EIS method. In terms of choosing the EECs, the relationship between $f_{\theta_{max}}$ and parameters proposes a new idea to identify the effectiveness of EECs.

Table 3. Relationship and calculated error of $f_{\theta_{max}}$ and R_c using Eq.(2) and Eq.(4)

Time	$f_{\theta_{max}}$	R_c	$\log(f_{\theta_{max}})$	Calculation	Error/%	Note
24h	0.5	299.50	-0.30	-0.31	1.95	Eq.(2)
48h	0.50	236.00	-0.30	-0.28	-6.30	
72h	0.07	243.9	-1.15	-1.05	-8.85	
96h	0.07	2.299	-1.15	-1.32	14.22	Eq.(4)
120h	0.07	2.672	-1.15	-1.36	17.43	
144h	0.07	2.419	-1.15	-1.20	3.74	
168h	0.02	0.486	-1.70	-2.01	18.46	

3.2 Analysis of glass transition temperature

Epoxy is widely used as the bottom base of 3PE coatings because of its high crosslinking density and good bonding strength with metal. However, its performance is greatly impacted by the glass transition temperature (T_g), which can be tested by a differential scanning calorimeter (DSC). The greater the degree of cure, the higher the T_g of the coating. In this study, the DSC is used to test the epoxy T_g in different cure time to identify the causes of delamination of 3PE coatings due to epoxy.

In this experiment, epoxy power was applied on test blocks using thermal spraying, and then the blocks were cooled at ambient temperature. The thickness was measured at five points, 4 corners and the center, on each sample every other day. The mean of the five measurements is taken to reflect the actual thickness of the specimens. DSC was conducted at 200°C in a nitrogen environment, and then is cooled down to the ambient temperature at the rate of 10°C/min.

As shown in Figure 5, it is obvious that the coating thickness and T_g first increase and then keep unchanged over time. On the fourth day, the T_g changes a little at 100°C, and in the following three days, it increases slightly to 105°C. The coating thickness shows the similar features. Therefore, the process of cure can be considered completed while T_g is 105°C and thickness is $33\pm 2\mu\text{m}$. At this moment, the epoxy is in a good condition with high crosslinking and adhesion [28].

The T_g of delaminated coating for the field use was tested, and the result is presented in Figure 6. As shown in the figure, T_g of the delaminated coating is much lower than that of the intact coating. It indicates that the coating delamination without defects is caused by the improperly cured coating. And the initiation of failure occurred may be the differential thermal expansion properties between the steel pipeline and epoxy power, enhanced by thermal cyclic fatigue loading due to the operation temperature, which may cause shrinkage stresses resulting in disbanded coating.

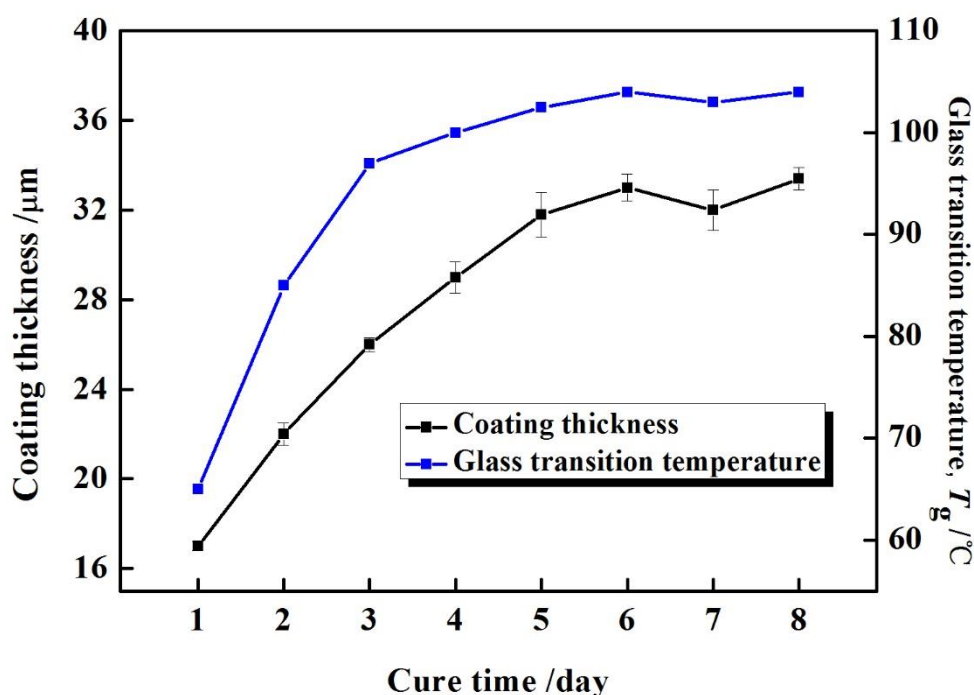


Figure 5. Coating thickness and T_g of single epoxy coating over cure time

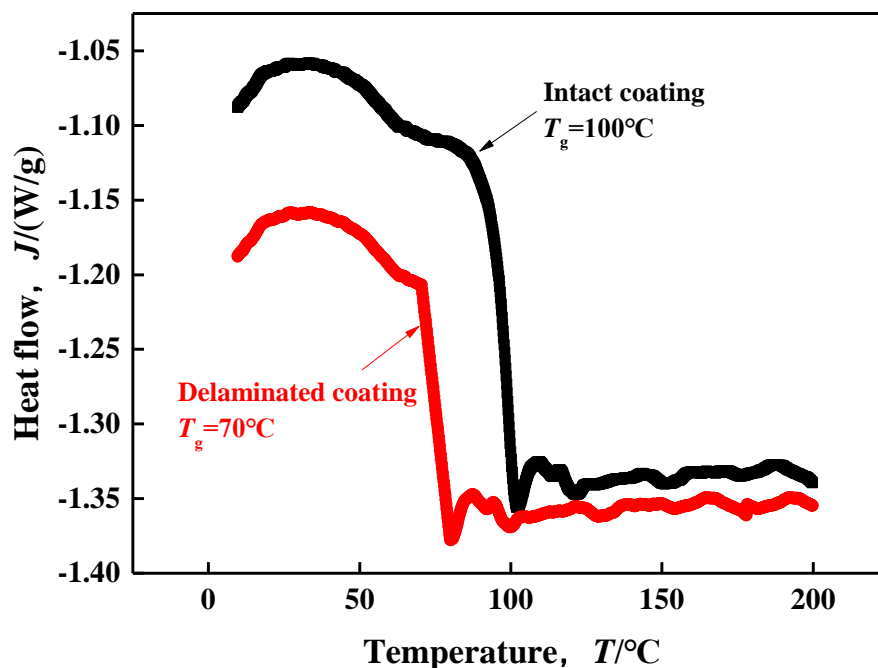


Figure 6. Results of DSC for coatings with/without delamination

4. CONCLUSIONS

In this paper, the causes of coating delamination are investigated, and the conclusions are drawn as follows:

(1) For the delaminated coatings with defects, the electrolyte diffusion on the coating and metal interface from the defects may result in delamination. The entire diffusion process can be divided into stages, formation of corrosive crevice, oxygen concentration corrosion, and hydrogen evolution.

(2) Delaminated coatings without defects could be caused by insufficient cure of epoxy, as a result of T_g lower than that of intact coatings.

(3) $f_{\theta_{max}}$ can be applied to evaluate the characteristic of coatings to study water permeation into coatings or investigate the failure process due to diffusion on the coating and metal interface,. Based on the physical meaning of EECs, the correlation between $f_{\theta_{max}}$ and all other parameters was established.

References

1. Z. Mahidashtia, T. Shahrabia and B. Ramezanzadehb, *Prog. Org. Coat.*, 144(2018)19.
2. Y.X. Xv, C.W. Yan, Y.M. Gao and C.N. Cao, *J. Ch. Soc. Corros. Protect.*, 22(2002) 58.
3. C.G. Oliveira and M.G.S. Ferreira, *Corros. Sci.*, 45(2003)123.
4. H.M. Tawancy, L.M. Al-Hadhrami, *J. Mater. Eng. Perform.*, 21(2012)1757.
5. X. Chen, X.G. Li, C.W. Du and Y.C. Cheng, *Corros. Sci.*, 51(2009)2242.
6. X. Liu, J. Xiong and Y. Lv, *Prog. Org. Coat.*, 2009,64: 497–503.
7. D.G. Lee, B.C. Kim, *J. Adhesion Sci. Technol.*, 19(2005)879.

8. A. Husain, S. Al-Bahar, J. Chakkamalayath, A. Vikraman, A. Al Ghamdi and T. Kamshad, *Eng. Fail. Anal.*, 56(2015)375.
9. M.J. Dai, J. Liu, F. Huang, Y.H. Zhang and Y.F. Cheng, *Corros. Sci.*, (2018).
10. J.C. Xu, Y. Jiang, T. Zhang, Y.T. Dai and P.F. Yang, *Prog. Org. Coat.*, 122(2018)10.
11. C. Yang, G. Cui, Z.L. Li, Y.L. Zhao and C.B. Zhang, *Int. J. Electrochem. Sci.*, 10(2015)10223.
12. M. Kendig, F. Mansfeld and S. Tsai, *Corros. Sci.*, 1983,23(4):317-329.
13. E.P.M. Van Westing, G.M. Ferrari and J.H.W. de Wit, *Corros. Sci.*, 39(1994)957.
14. C. Pérez, A. Collazo, M. Izquierdo, P. Merino and X. R. Novoa, *Prog. Org. Coat.*, 36(1999)102.
15. J.W. Oldfield and W.H. Sutton, *Br. Corros. J.*, 13(1978)13.
16. J.W. Oldfield and W.H. Sutton, *Br. Corros. J.*, 13(1989)104.
17. A. Husain, J. Chakkamalayath and S. Al-Baha, *Eng. Fail. Anal.*, 82(2017)765.
18. H.W. Pickering and R.P. Frankenthal, *J. Electrochem. Soc.*, 119(1972)1297.
19. H.W. Pickering and R.P. Frankenthal, *J. Electrochem. Soc.*, 119(1972)1304.
20. C.F. Zhu, R. Xie, J.H. Xue and L.L. Song, *Electrochim. Acta*, 56(2011)5828.
21. A. Husain and A. Fakhraldeen, *Desalination*, 158(2003)29.
22. S. Touzain, *Electrochim. Acta*, 55(2010)6190.
23. N.J.W. Reuvers, H.P. Huinmink, O.C.G. Adan, S.J. Garcia and J.M.C. Mol, *Electrochim. Acta*, 94(2013)219.
24. X.D. Yan, J.M. Gao and Y.P. Wang, *Modern Paint & Finishing*, 2010,13(6):30-33.
25. E. Akbarinezhad, F. Rezaei and J. Neshati, *Prog. Org. Coat.*, 61(2018)45.-52.
26. J. Liu, L.W. Zhang and X.L. Mu, *Prog. Org. Coat.*, 111 (2017) 315.
27. V.B. Gupta and C. Brahatheeswaran, *Polymer*, 32(1991)1875.
28. J.B. Enns and J.K. Gillham, *J. Appl. Polym. Sci.*, 28(1983)2831.

© 2019 The Authors. Published by ESG (www.electrochemsci.org). This article is an open access article distributed under the terms and conditions of the Creative Commons Attribution license (<http://creativecommons.org/licenses/by/4.0/>).